High-pressure study of $ScVO_4$ by Raman scattering and *ab initio* calculations

V. Panchal[1,*], F.J. Manjón[2,*], D. Errandonea[1,*,†], P. Rodriguez-Hernandez[3,*], J. López-Solano[3,*], A. Muñoz[3,*], S. N. Achary[4], and A. K. Tyagi[4]

[1] Departamento de Física Aplicada-ICMUV, Universidad de Valencia, Edificio de Investigación, C/Dr. Moliner 50, 46100 Burjassot (Valencia), Spain

[2] Instituto de Diseño para la Fabricación y Producción Automatizada, Universidad Politécnica de Valencia, Camino de Vera s/n, 46022 Valencia, Spain

[3] Departamento de Física Fundamental II, Instituto de Materiales y Nanotecnología, Universidad de La Laguna, La Laguna 38205, Tenerife, Spain

[4] Chemistry Division, Bhabha Atomic Research Centre, Trombay, Mumbai 400085, India

We report results of experimental and theoretical lattice-dynamics studies on scandium orthovanadate up to 35 GPa. Raman-active modes of the low-pressure zircon phase are measured up to 8.2 GPa, where the onset of an irreversible zircon-to-scheelite phase transition is detected. Raman-active modes in the scheelite structure are observed up to 16.5 GPa. Beyond 18.2 GPa we detected a gradual splitting of the E_g modes of the scheelite phase, indicating the onset of a second-phase transition. Raman symmetries, frequencies, and pressure coefficients in the three phases of $ScVO_4$ are discussed in the light of *ab initio* lattice-dynamics calculations that support the experimental results. The results on all the three phases of $ScVO_4$ are compared with those previously reported for related orthovanadates.

PACS numbers: 62.50.+p, 63.20.-e, 78.30.-j, 71.15.Mb

[*] Member of the MALTA Consolider Team

[†] Corresponding author; email: daniel.errandonea@uv.es

I. Introduction

Orthovanadates with composition AVO_4 (A = trivalent metal) with pentavalent vanadium are found in numerous applications due to their interesting magnetic, optical, and electronic properties. In addition to their wide practical applicability, these materials are also commonly used as cathodoluminescent, thermophosphors, scintillators, photocatalysis materials and in lithium ion batteries [1, 2]. As a consequence of the extravagant applications of orthovanadates in last few years they have been extensively investigated under high-pressure (HP), like other ABO_4 compounds, in order to understand their mechanical properties and HP structural phase transitions [3].

$ScVO_4$ crystallizes in tetragonal zircon-type structure (space group: $I4_1/amd$, Z = 2) at ambient conditions. In this structure, the vanadium atom is tetrahedrally coordinated while the trivalent metal is octahedrally coordinated to oxygen atoms [4]. Recent x-ray diffraction (XRD) measurements on $ScVO_4$ have shown the onset of a non-reversible structural phase transition from the low-pressure zircon-type structure to a denser scheelite-type structure (space group: $I4_1/a$, Z = 4) at 8.7 GPa [5]. *Ab initio* calculations confirmed this transition (at 5.8 GPa) and predicted the existence of a second one at 9 GPa [6]. However, XRD measurements found the scheelite-type structure to be stable up to 27 GPa. Similar discrepancies were observed earlier in isomorphic YVO_4 and were resolved by the combination of HP Raman measurements and lattice-dynamics calculations [7]. To the best of our knowledge, there is no HP Raman study of $ScVO_4$ reported yet. Here, we report Raman scattering measurements in $ScVO_4$ up to 35 GPa together with *ab initio* lattice-dynamics calculations. Our purpose is to assign the symmetry of the Raman modes in the zircon and scheelite phases of $ScVO_4$ and to explore the possible scheelite-to-fergusonite transition as theoretically predicted.

Further, we will compare and discuss the results on $ScVO_4$ with those of other orthovanadates and orthophosphates.

II. Experimental details

$ScVO_4$ samples used in the experiments were prepared by solid state reaction of appropriate amounts of predried Sc_2O_3 (Indian Rare Earth Ltd. 99%) and V_2O_5 (Alfa-Aesar 99%). Homogeneous mixtures of the reactants were pelletized and heated at 800°C for 24 h and then cooled to room temperature. Further, the pellets were reground and heated again at 1100°C for 24 h. The sample obtained was characterized by powder x-ray diffraction recorded on a Philips X-pert Pro diffractometer using Cu K_α radiation. Single phase of $ScVO_4$ of zircon-type structure was confirmed with structural parameters identical to those reported in Ref. [5].

The prepared powder sample of $ScVO_4$, along with a 2-μm diameter ruby ball, was loaded in a pre-indented steel gasket with a 200-μm diameter hole inside a diamond-anvil cell. A 4:1 methanol-ethanol mixture was used as pressure-transmitting medium [8, 9]. The pressure was determined by monitoring the shift in ruby fluorescence lines [10]. HP Raman measurements were performed in the backscattering geometry using 632.8 nm HeNe laser and a Horiba Jobin Yvon LabRAM HR UV microspectrometer in combination with a thermoelectric-cooled multichannel CCD detector with spectral resolution below 2 cm^{-1}. Three experimental runs were carried out with similar results.

III. Lattice dynamics calculations

The calculations reported here have been performed using the formalism of density-functional theory (DFT). In particular, the Vienna simulation package VASP (see Refs. 11, 12 and references therein) has been used to perform structural

calculations with the pseudo-potential method. The set of plane waves employed extended up to a kinetic energy cutoff of 540 eV, such a large cutoff was required to achieve highly converged results within the projector augmented wave (PAW) scheme [13, 14] The PAW method takes into account the full nodal character of all the electron charge density distribution in the core region. The exchange-correlation energy was initially taken in generalized-gradient approximation (GGA) with the Perdew-Burke-Ernzerhof (PBE) prescription [15]. We used a dense grid of k-special points for integrations along the Brillouin zone (BZ) in order to assure highly converged results to about 1-2 meV per formula unit yielding accurate and well converged forces. At each selected volume, the structures were fully relaxed to their equilibrium configuration through the calculation of the forces on atoms and the stress tensor [16]. In the relaxed equilibrium configuration, the forces are less than 0.004 eV/Å and the deviation of the stress tensor from a diagonal hydrostatic form is less than 0.2 GPa. Lattice-dynamics calculations of phonon modes were performed in zircon, scheelite and fergusonite structures at the zone centre (Γ point) of the BZ. The calculations provided information about the frequency, symmetry and polarization vector of the vibrational modes in each structure. Highly converged results on forces are required for the calculation of dynamical matrix of lattice-dynamics calculations. We use direct force-constant approach (or supercell method) [17]. The construction of the dynamical matrix at the Γ point of the BZ is particularly simple and involves separate calculation of the forces in which a fixed displacement from the equilibrium configuration of the atoms within the primitive unit cell is considered. Symmetry further reduces the computational efforts by reducing the number of such independent displacements in the analyzed structures. Diagonalization of the dynamical matrix provides both the frequencies of the normal

modes and their polarization vectors. It allows us to identify the irreducible representations and the character of phonon modes at the Γ point.

IV. Results

A. Zircon-structured $ScVO_4$

At ambient conditions, $ScVO_4$ exists in the zircon structure (space group: $I4_1/amd$, point group D_{4h}) with two formula units per primitive cell. The group theoretical analysis predicts 12 first-order Raman-active modes at the center of the BZ with symmetries $\Gamma = 2A_{1g} + 4B_{1g} + B_{2g} + 5E_g$ [18]. These modes can be further classified into internal (ν_1-ν_4) and external (translational, T, and rotational, R) modes of VO_4 units as follows,

$$\Gamma = A_{1g}(\nu_1, \nu_2) + B_{1g}(2T, \nu_3, \nu_4) + B_{2g}(\nu_2) + E_g(2T, R, \nu_3, \nu_4). \quad (1)$$

Figure 1(a) shows the Raman spectra of $ScVO_4$ in the zircon phase at different pressures up to 7.6 GPa. The Raman spectrum in orthovanadates can be divided into two regions [7, 18-19]. The high-frequency region (800-950 cm^{-1}) comprises the region where the symmetric-stretching mode $\nu_1(A_{1g})$ and the asymmetric-stretching modes $\nu_3(E_g)$ and $\nu_3(B_g)$ are observed. The low frequency region (250-500 cm^{-1}) comprises the region of the bending modes. At ambient conditions 10 out of the 12 first-order Raman peaks are clearly discernable. Apart from these first-order Raman modes we have observed three additional peaks in the frequency gap of 500-800 cm^{-1} (marked by asterisks in **Figure 1(a)**). They are likely to be second-order Raman modes. The symmetry assignment for the first-order modes has been performed in accordance with our calculations and comparison with previous results in other vanadates and it is summarized in **Table I**.

Regarding the analysis of the Raman spectra of the zircon phase, it can be noted that the intense symmetric-stretching internal mode $\nu_1(A_{1g})$, observed at 914 cm^{-1} at ambient pressure (10^{-4} GPa), is the highest in frequency among the family of orthovanadates [20]. This indicates that $ScVO_4$ exhibits the strongest intra-tetrahedral V-O bonds among orthovanadates. Apart from this mode, we have observed two asymmetric-stretching modes $\nu_3(E_g)$ and $\nu_3(B_{1g})$ at 826 and 817 cm^{-1}, respectively. Note that in $ScVO_4$, as in other vanadates [5, 20], ν_1 has a higher frequency than ν_3. However, this relation becomes opposite (i.e. $\nu_1 < \nu_3$) in $ScPO_4$ [21]. This difference is due to the increase in covalence on the V-O bond resulting from the shift of the energies of the V 3d states relative to the O 2p valence band [22]. Regarding the other phonons of $ScVO_4$, out of 4 bending modes of the VO_4 unit we could observe only 3 modes: $\nu_4(B_{1g})$ at 494 cm^{-1}, $\nu_4(A_{1g})$ at 356 cm^{-1} and $\nu_2(B_{2g})$ at 263 cm^{-1}. The asymmetric-bending mode $\nu_4(E_g)$ could not be detected. Similarly, one of the external translational $T(B_{1g})$ modes has not been detected. In most of the Raman measurements in orthovanadates these two modes are absent probably due to their weak Raman scattering cross-section [20].

Figure 1(b) shows the pressure dependence of Raman modes in the zircon phase. The symmetry assignment for the Raman modes along with their experimental and calculated frequencies, pressure coefficients, and mode Grüneisen parameters (γ) are shown in **Table I**. Agreement between experimental and calculated frequencies and pressure coefficients for the Raman modes is rather good. The Grüneisen parameters of the different modes in the zircon phase have been obtained by using the bulk modulus B_0 = 178 GPa reported earlier by XRD measurements on $ScVO_4$ [5].

The frequencies of the Raman modes of the zircon phase were found to increase with increasing pressure except for the external $T(E_g)$ mode at 165 cm^{-1} and the internal $\nu_2(B_{2g})$ mode at 263 cm^{-1} at ambient pressure that exhibit negative pressure coefficients.

A similar behavior was observed for other orthovanadates, e.g. YVO_4 [7], $YbVO_4$ [19] and $LuVO_4$ [23] and also in $ScPO_4$ [21]. This softening of the two modes seems to be a characteristic behavior of zircon-type compounds that can be considered as a precursor of a phase transition upon compression [7, 19, 23, 24]. The pressure coefficient of the $\nu_2(B_{2g})$ bending mode, assigned in other works as the $T(E_g)$ or $T(B_g)$ modes, is found to be similar among orthovanadates and of the order of -1.2 to - 1.4 cm^{-1}/GPa [7, 19, 23, 24]. On the other hand, the pressure coefficient of the $T(E_g)$ mode with the lowest frequency is very small (-0.05 cm^{-1}/GPa) for $ScVO_4$ and is similar in the case of YVO_4 [7], while it is a little bit larger for other compounds [19, 23]. Softening of $T(E_g)$ and $\nu_2(B_{2g})$ modes in zircon-type compounds evidence an induced distortion in the zircon structure responsible for zircon-to-scheelite transition. In general, we have found very similar pressure coefficients for the Raman mode frequencies in orthovanadates; e.g., the pressure coefficients for the internal stretching modes and the highest frequency $T(E_g)$ mode are found to be of the order of 5.2 to 6.4 cm^{-1}/GPa. To close this description of the pressure evolution of Raman phonons we would like to add that the rotational $R(E_g)$ mode of $ScVO_4$ has the largest pressure coefficient (see **Table I**). The same large pressure coefficient is observed for this mode in $ScPO_4$ [21] and indicates a strengthening of the Sc - VO_4 bonds with compression. This result suggests that the small Sc^{3+} cation leads to a tension of VO_4 units in the zircon phase that does not favor the rotation of the VO_4 units around the c axis. Furthermore, on increasing pressure the decrease of the Sc^{3+} ionic radius makes this effect even stronger. On the contrary, zircon-type AVO_4 compounds with an *A* cation with larger ionic radius than Sc, like rare earths, would tend to facilitate the rotation of the VO_4 units leading to smaller pressure coefficients for the rotational mode.

From the knowledge of stretching mode frequencies of orthovanadates we can estimate the Pauling's bond strength, also referred as bond valence, of V-O bonds. The general relation between stretching mode frequency and bond length R (in Å) in the vanadium oxides is given as [25],

$$\omega\ (cm^{-1}) = 21349 \exp(-1.9176R) \quad (2)$$

There exists a relationship between the bond length R (Å) and the Pauling bond strength S, which is given as [26],

$$S_{V\text{-}O} = (R / 1.791)^{-5.1} \quad (3)$$

Here, $S_{V\text{-}O}$ is expressed in the valence units (v.u.), and one valence unit corresponds to 1.791 Å in bond length. The observed stretching frequencies of VO_4 units in zircon phase $ScVO_4$ are 914.2, 856.5 and 817.1 cm^{-1}, respectively. The corresponding bond lengths using equation (2) are 1.64, 1.68, and 1.70 Å, respectively and the three bond strengths using equation (3) are 1.55, 1.39, and 1.29 v.u., respectively. Adding these bond strengths by counting twice the contribution from shortest bond length on account of fourfold coordination in VO_4 we can estimate the total valence of 5.52 v.u., which is close but higher than the valence of V^{+5} ion. A similar overestimation of the total valence of V in the zircon phase was also recently found for YVO_4 [7].

B. Scheelite-structured $ScVO_4$

As already mentioned, recent XRD measurements in $ScVO_4$ show that it undergoes a zircon-to-scheelite phase transition around 8.7 GPa [5]. This value is somewhat higher than that obtained from theoretical calculations (5.8 GPa) [6]. Group theoretical calculations for $ScVO_4$ in scheelite phase (space group: $I4_1/a$, point group C_{4h}^6) predict 13 first-order Raman modes at the BZ centre with following symmetries Γ

= $3A_g + 5\ B_g + 5\ E_g$ [27]. These modes can be further classified either as internal (ν_1 to ν_4) or external (T and R) modes of the VO_4 units,

$$\Gamma = \nu_1(A_g) + \nu_2(A_g) + \nu_2(B_g) + \nu_3(B_g) + \nu_3(E_g) + \nu_4(B_g) + \nu_4(E_g) +$$
$$+ R(A_g) + R(E_g) + 2T(B_g) + 2T(E_g) \quad (4)$$

Raman spectra of $ScVO_4$ in the scheelite phase are shown in **Figure 2(a)**. Around 8.2 GPa we have observed an appearance of the two extra Raman bands at 183cm^{-1} and 283cm^{-1}, these two modes are assigned as $T(E_g)$, and $\nu_2(A_g)$ modes of scheelite phase indicating the onset of zircon-to-scheelite phase transition. At higher pressures, we observed the appearance of many Raman bands, as showed by arrows in **Figure 2(a)** - accompanied by broadening of Raman modes. A weak presence of the Raman modes of the zircon phase can be detected up to 15.1 GPa. The coexistence of the low- and high-pressure phases is consistent with XRD studies [5]. A typical feature of the transition is that the frequency of symmetric stretching mode $\nu_1(A_g)$ drops abruptly across it. These changes in the Raman spectra are indicative of a structural phase transition towards the lower-symmetry tetragonal scheelite phase, as already observed in other orthovanadates [7, 19, 23, 24]. Out of 13 Raman-active modes in the scheelite phase, we observed only 11 modes with measurable intensity up to 16.5 GPa. Above this pressure changes in the Raman spectra point towards a possible second phase transition which will be discussed in the next section.

The mode assignment of the experimentally observed Raman modes in $ScVO_4$ in the scheelite phase was done according to our calculations and is shown in **Table II**. The highest frequency mode at 826 cm^{-1} is assigned to the symmetric stretching mode $\nu_1(A_g)$ and its frequency is observed to be approximately similar in the scheelite phase of other ortovanadates, like YVO_4, $YbVO_4$, $DyVO_4$, and $TbVO_4$ irrespective of V-O bond distance [7, 19, 24]. This behavior is completely different to what is observed in

the zircon phase, where the highest-frequency mode scales with the V-O bond distance in the different vanadates. The different behaviors of the symmetric-stretching modes in zircon and scheelite phases will be addressed in the discussion section. The other two asymmetric-stretching modes of the scheelite phase of $ScVO_4$ are observed near 760 and 726 cm^{-1} and assigned to $\nu_3(E_g)$ and $\nu_3(B_g)$ modes, respectively. The four bending vibrations are observed experimentally at 456, 449, 363, and 257 cm^{-1} and assigned to the $\nu_4(E_g)$, $\nu_4(B_g)$, $\nu_2(B_g)$, and $\nu_2(A_g)$ modes, respectively. Additionally, we could observe 4 out 6 external modes predicted for scheelite phase till the highest pressure attained in our experiment (see **Fig. 2(a)**). The external translational mode of $T(B_g)$ symmetry with the lowest frequency could not be detected likely due to its weak intensity and the fact that, according to our calculations, it is very close to the intense $T(E_g)$ mode. Curiously, our calculations have predicted the softening of this $T(B_g)$ mode which we have not been able to measure. Similarly, the rotational $R(A_g)$ mode, deriving from the silent rotational $R(A_g)$ mode of the zircon phase, could not be detected due to its weak intensity. In general, the calculated Raman frequencies are in good agreement with our experimental frequencies with maximum deviation of 7.5%. The same agreement of experiment and calculations holds for the Raman frequency pressure coefficients. All these data are shown in **Table II** together with mode Grüneisen parameters (γ), calculated using the bulk modulus of the scheelite phase, B_0 = 210 GPa, as reported in Ref. 5.

Figure 2(b) shows the pressure evolution of the Raman modes of $ScVO_4$ in the scheelite phase. As mentioned earlier, our calculations indicate the softening of the external $T(B_g)$ mode of the lowest frequency in the scheelite phase with increasing pressure with a very small pressure coefficient (-0.19 cm^{-1}/GPa). A similar softening of this $T(B_g)$ mode was predicted by lattice-dynamics calculations and indeed

experimentally found in YVO_4 [7]. However, the softening of the lowest-frequency $T(B_g)$ Raman mode has not been reported in the studies published on $YbVO_4$ [19], $LuVO_4$ [23 28], $TbVO_4$, and $DyVO_4$ [24]. Curiously, a similar softening of the lowest-frequency $T(B_g)$ mode is frequently observed in the family of scheelite tungstates and molybdates that undergo a scheelite-to-fergusonite transition [29 - 31].

We can estimate the Pauling's bond strength of $ScVO_4$ in the scheelite phase by taking into account the stretching-mode frequencies in a similar way as earlier calculated for the zircon phase. The observed stretching mode frequencies in the scheelite phase of $ScVO_4$ are 826.1, 760.9 and 727.5 cm^{-1} at ambient pressure, respectively. The corresponding bond lengths using equation (2) are 1.70, 1.74, and 1.76 Å, respectively, and the three corresponding bond strengths obtained by using equation (3) are 1.31, 1.16, and 1.09 v.u., respectively. Summing these bond strengths by counting twice the contribution from shortest bond length on account of four fold co-ordination in VO_4 we can estimate the total valence of 4.65 v.u., which is close to valence of V^{+5} ion. A similar value for the total valence of V^{+5} ion was obtained for YVO_4 at ambient pressure in Ref. 7. The value of the bond strength in the scheelite phase is quite small as compared to zircon phase (5.52 v.u. at ambient pressure). Since the bond strength should be around 5 and taking into account that it increases with increasing pressure we can consider that the scheelite phase is a very stable phase while the high value of bond strength in the zircon phase could be indicative of the instability of zircon phase, as already pointed out in Ref. 7. In this sense, **Figure 2(a)** shows the Raman spectra of $ScVO_4$ on downstroke from 16.5 GPa till ambient pressure. It can be observed that on release of pressure the scheelite phase does not revert back to the zircon phase, thus evidencing the irreversible nature of the zircon-to-scheelite phase transition and the metastable character of the scheelite phase at ambient conditions.

C. Fergusonite-structured $ScVO_4$

As already commented, a scheelite-to-fergusonite phase transition has been observed in a number of orthovanadates and our theoretical calculations for $ScVO_4$ suggests a scheelite-to-fergusonite phase transition above 9 GPa [6]. Group theoretical calculations for $ScVO_4$ in the fergusonite phase (space group: *I2/a*, point group C_{2h}^6) predict 18 first-order Raman modes near the BZ centre with following symmetries, $\Gamma = 8A_g + 10\ B_g$. The correlation between the scheelite and fergusonite Raman modes is as follows: every A_g and B_g scheelite mode converts into an A_g mode of the monoclinic symmetry while every doubly degenerate E_g mode converts into two B_g modes.

Figure 3 shows the Raman spectra of $ScVO_4$ from 16.5 GPa to 35 GPa. Beyond 18.2 GPa we have observed noticeable changes in the Raman spectra. In particular, both the $\nu_3(E_g)$ mode at 540 cm^{-1} and $\nu_4(E_g)$ mode at 770 cm^{-1} (marked with arrows in **Fig. 3**) of scheelite-type $ScVO_4$ show a considerable broadening. We have interpreted these broadenings as associated with the splitting of E_g modes into two B_g modes in the fergusonite phase beyond 18.2 GPa (see arrows in **Fig. 3**). Raman measurements in orthovanadates, YVO_4, $YbVO_4$, and $LuVO_4$ also report such splitting of E_g modes [7, 19, 23] and the same holds for scheelite tungstates $BaWO_4$ and $PbWO_4$ [29, 30]. Furthermore, lattice-dynamics calculations for the fergusonite phase are in good agreement with the experimental results. The splitting of E_g modes could only be observed for the V-O stretching modes. Among the external E_g modes the splitting could not be detected. A similar behavior was observed in case of $YbVO_4$ and $LuVO_4$ [19, 23]. Hence, to fully understand the observed changes in the Raman spectra at 18.2 GPa, we have analyzed full-width half maxima (FWHM) of $\nu_3(E_g)$ mode [as it is relatively broad and intense compared to $\nu_4(E_g)$ mode] at various pressures and shown in **Figure 4**. The experimentally evident discontinuity in FWHM beyond 18.2 GPa

supports the splitting of $\nu_3(E_g)$ mode and hence indicates scheelite-to-fergusonite transition occurs around this pressure. The mode assignment of all the Raman modes in fergusonite-type $ScVO_4$ is done according to our calculations. **Table III** summarizes the theoretical and experimental Raman mode frequencies and pressure coefficients in fergusonite $ScVO_4$ at 23.3 and 23.4 GPa, respectively. The experimental and calculated Raman frequencies and pressure coefficients are in good agreement thus supporting the observation of the scheelite-to-fergusonite transition.

It should be noted that there is no discontinuity in the volume across the scheelite-to-fergusonite phase transition because it is a displacive second-order phase transition. Therefore, Raman modes do not show a measurable discontinuity across scheelite-to-fergusonite transformation as it has been observed in many orthovanadates like YVO_4, $YbVO_4$ and $LuVO_4$ [7, 19, 23]. **Figure 2(b)** show the pressure dependence of $ScVO_4$ in the fergusonite phase between 18.2 to 35 GPa. It can be observed that on release of pressure the fergusonite phase was detected until 11 GPa where it transforms back to the scheelite phase. This fact is consistent with the theoretical results, which predict for both transitions a transition pressure smaller (9 GPa) than the experimental value.

To close this section we would like to comment on the fact that XRD studies did not detected the scheelite-to-fergusonite transition. The causes can be multiple. First, the use of different pressure media could strongly affect the structural sequence of ternary oxides like $ScVO_4$ [32]. Second, Raman measurements are more sensitive to subtle phase transitions than XRD [33]. In particular, in the case of a second-order transition involving only gradual distortions like the scheelite-to-fergusonite transition. This transition induces important changes in the Raman spectrum (the active modes increase from 13 to 18) but only slight changes in XRD patterns [34, 35]. Finally, the broadening

induced by pressure in Bragg peaks [5, 36] could mask the onset of the transition. Indeed XRD experiments did not detect the same transition in YVO_4 whereas Raman experiments did it [7]. New HP XRD experiments, using a pressure medium like He or Ne, are needed to further investigate the scheelite-to-fergusonite transition in $ScVO_4$ and YVO_4.

D. Discussion

Concerning to the structural sequence in zircon-type ABO_4 compounds, it is known that many of them transform to the scheelite phase and then to the fergusonite phase [3]. The zircon-to-scheelite phase transition is a first-order reconstructive phase transition with a probable coexistence of both phases over a wide pressure range [37] and it has been observed in phosphates [20, 38], chromates [39, 40], vanadates [5, 22, 23, 24], germanates [41], and silicates [37, 42]. On the other hand, the scheelite-to-fergusonite transition is a second-order displacive transition involving a smooth transition across the transition pressure [43, 44] and it has been reported in tungstates [45, 46] and molybdates [34]. In the case of orthovanadates, the complete sequence of structural transformations was previously observed in $LuVO_4$ [23], $EuVO_4$ [5], $YbVO_4$ [19], and $LuVO_4$ [24]. The second phase transition in $ScVO_4$, namely from scheelite-to-fergusonite, has been detected beyond 18.2 GPa in agreement with our total-energy calculations prediction. This pressure is similar to the theoretical pressure for the scheelite-to-fergusonite phase transition in YVO_4 (19 GPa) [7].

Since the scheelite-to-fergusonite transition is ferroelastic displacive in nature [43], it is expected that there exist an order parameter involving a slight distortion of tetrahedra (tilt or displacement) which is adequate to trigger such transitions. Recently, the presence of a soft $T(B_g)$ mode has been related to the existence of the scheelite-to-

fergusonite transition in scheelite-type molybdates and tungstates [39]. We could not detect this $T(B_g)$ mode in scheelite phase, but our lattice dynamics calculations predict the softening of the lowest-frequency $T(B_g)$ Raman mode in $ScVO_4$, as it was observed in YVO_4 [7]; thus suggesting that the scheelite-to-fergusonite transformation could be expected in both compounds. In fact, the scheelite-to-fergusonite phase transition in YVO_4 was predicted near 19 GPa but was not clearly observed until 24 GPa [7]. In this respect, we want to point out that the scheelite-to-fergusonite phase transition has been observed in many rare-earth orthovanadates despite a soft $T(B_g)$ mode has not been observed in them. At present, we have no explanation for this fact, which implies that the $T(B_g)$ mode softening cannot be regarded as the order parameter involved in the scheelite-to-fergusonite transition in many orthovanadates. In order to clarify this subject, more work is needed.

Zircon-type AVO_4 compounds with a trivalent metal from the lanthanide series show a reduction of the lattice constants and of the A-O and V-O bond distances on decreasing the rare-earth radius. The decrease of the A-O bond length in going from La to Lu is 6% while the V-O bond distance decreases by 0.2%. This small reduction of the V-O bond distance results in an increase of the force constant and consequently leads to a small increase of the symmetric stretching frequency $\nu_1(A_{1g})$ in the zircon phase, as already commented [47, 48]. However, it is interesting to observe that the frequency of the symmetric stretching mode $\nu_1(A_g)$ in the scheelite phase remains constant irrespective of the *A* cation radius. **Figure 5a** shows the stretching Raman mode frequencies in both zircon and scheelite phases for different orthovanadates at ambient pressure as a function of the ionic radius of the *A* cation [7, 19, 20, 23, 24, 49 – 54]. The data corresponding to **Figure 5a** are summarized in **Table IV**. Note that the

described behavior is followed not only for rare-earth orthovanadates, but also to the rest of members of the orthovanadate family.

The present behavior for the symmetric-stretching mode has not been found in other scheelites [29] and it suggests that there is no change in the force constant of the V-O bond in the scheelite phase of orthovanadates despite the reduction of the lattice parameters on decreasing the *A* cation radius. The dependence of the force constant with *A* cation in zircon-type vanadates and the invariability of the force constant in scheelite-type vanadates could be understood on the light of the symmetry of the tetragonal zircon and scheelite phases. The scheelite structure is characterized by a setting angle whose value could be between 0 and 45º; these are the limit values at which the scheelite structure adopt the more rigid and higher symmetry zircon structure [55]. Therefore, the scheelite structure can vary the lattice constant on changing the *A* cation by varying the setting angle but without reducing the V-O bond distance. In this way, the flexible scheelite structure can accommodate different *A* cations with decreasing ionic radii by increasing the setting angle without varying the V-O distance. This is not possible in the higher symmetry zircon phase where the rotation of VO_4 tetrahedra is not allowed and consequently decreasing *A* ionic radii leads to a reduction of the V-O bond distance.

In summary, VO_4 tetrahedra are more symmetric and densely packed in the scheelite phase than in the zircon phase due to the tetrahedral tilting available in the less symmetric tetragonal scheelite phase compared to the rigid zircon phase. Consequently, the change of *A* cation radius in scheelite orthovanadates does not result in a change in V-O bond distance neither in a change of the V-O force constant but in a different setting angle for each compound. On the contrary, the rigid VO_4 tetrahedra of the zircon

phase cannot rotate and must change V-O bond distance. Consequently, the V-O force constant depends upon the *A* cation radius.

Furthermore, we have noted a dependence of the zircon-to-scheelite phase transition pressure in AVO_4 compounds on the *A* ionic radius (see **Fig. 5 (b)**). **Table V** summarizes the zircon-to-scheelite transition pressures (obtained from Raman experiments) as a function of the ionic radius of the *A* cation. The higher the ionic radius is, the lower the phase-transition pressure. This result is directly related to the position of the orthovanadates at the Bastide's diagram [3] and is in good agreement with the observation that orthovanadates with large *A* ionic radii can be also crystallized either in the scheelite ($BiVO_4$) [56] or in the monazite ($LaVO_4$) [57] phase. Summarizing, these results indicate that the zircon phase is more stable in compounds with a small ionic radius of the *A* cation. According with this conclusion, $ErVO_4$ and $HoVO_4$ are predicted to undergo phase transitions near 7 GPa, $EuVO_4$ and $SmVO_4$ at 6 GPa, and $PrVO_4$ at 5 GPa. The prediction made for $EuVO_4$ is consistent with the results obtained in XRD measurements [5], where the transition pressure is slightly larger as found in other vanadates when XRD and Raman studies are compared.

Finally, we should mention that according to our estimations of bulk moduli in scheelite-type compounds [58], the compressibility of scheelite-type AVO_4 compounds is directly related to the compressibility of the AO_8 polyhedra due to the rather uncompressible VO_4 tetrahedra. Therefore, $ScVO_4$ should have the least volume among the orthovanadates due to the small ionic radius of Sc and a very high bulk modulus due to the high incompressibility of the ScO_8 polyhedra. Recent HP XRD measurements support our arguments [5].

V. Conclusions

Our combined experimental and theoretical study of scandium orthovanadate up to 35 GPa suggests that the low-pressure zircon phase undergo irreversible zircon to scheelite phase transition above 8.2 GPa. Beyond 18.2 GPa the $\nu_4(E_g)$ and $\nu_3(E_g)$ scheelite modes show a gradual splitting indicating the onset of scheelite-to-fergusonite phase transition. On release of pressure the fergusonite phase was detected down to 11 GPa. Below 11 GPa the sample retains the metastable scheelite phase even at ambient pressure. The symmetries of the Raman modes in the zircon, scheelite, and fergusonite phases of $ScVO_4$ have been assigned thanks to our lattice dynamics calculations. In general, a good agreement is found between our experimental and theoretical data.

We have evidenced and discussed a notable dependence of the symmetric stretching mode frequencies with the radius of *A* cation in AVO_4 compounds in the zircon phase unlike in the scheelite phase. Similarly, a considerable dependence of the zircon-to-scheelite transition pressure and of the bulk compressibility of the zircon phase on the *A* cation ionic radius is evidenced. Additionally, we have noted a lack of a soft mode behavior in some scheelite-type rare-earth orthovanadates, unlike $ScVO_4$ and YVO_4. All these results deserve a deeper analysis of the HP behavior of orthovanadates that we hope to stimulate with this work.

Aknowledgements

We acknowledge the financial support of the Spanish MCYT under Grant Nos. MAT2007-65990-C03-01/03, MAT2010-21270-C04-01/03/04, and CSD2007-00045, and the computation time provided by the Red Española de Supercomputación and the supercomputer Atlante. F.J.M. acknowledges also financial support from "Vicerrectorado de Innovación y Desarrollo de la UPV" (PAID-05-2009 through project UPV2010-0096).

References

[1] S. P. Shafi, M. W. Kotyk, L. M. D. Cranswick, V. K. Michaelis, S. Kroeker, and M. Bieringer, Inorganic Chemistry **48**, 10553 (2009) and references therein.

[2] D. F. Mullica, E. L. Sappenifield, M. M. Abraham, B. C. Chakoumakos, and L. A. Boatner, Inorg. Chim. Acta **248**, 85 (1996).

[3] D. Errandonea, and F. J. Manjón, Prog. Mater. Sci. **53**, 711 (2008).

[4] T. Aldred, Acta Crystallogr. **B 40**, 569 (1984).

[5] D. Errandonea, R. Lacomba-Perales, J. Ruiz-Fuertes, A. Segura, S. N. Achary, and A. K. Tyagi, Phys. Rev. **B 79**, 184104 (2009).

[6] J. López-Solano, P. Rodríguez-Hernández, and A. Muñoz, High Pressure Research **29**, 582 (2009).

[7] F. J. Manjón, P. Rodríguez-Hernández, A. Muñoz, A. H. Romero, and D. Errandonea, Phys. Rev. **B 81**, 075202 (2010).

[8] S. Klotz, L. Paumier, G. Le Marchand, and P. Munsch, J. Phys. D: Appl. Phys. **42**, 075413 (2009).

[9] D. Errandonea, Y. Meng, M. Somayazulu, and D. Häusermann, Physica **B 355**, 116 (2005).

[10] H. K. Mao, J. Xu, and P. M. Bell, J. Geophys. Res. **91**, 4673 (1986).

[11] G. Kresse, and J. Furthmüller, Phys. Rev. **B 54**, 11169 (1996).

[12] G. Kresse, and D. Joubert, Phys. Rev. **B 59**, 1758 (1999).

[13] P. E. Blöchl, Phys. Rev. **B 50**, 17953 (1994).

[14] G. Kresse, and D. Joubert, Phys. Rev. **B 59**, 1758 (1999).

[15] J. P. Perdew, S. Burke, and M. Ernzerhof, Phys. Rev. Lett. **77**, 3865 (1996).

[16] A. Mujica, A. Rubio, A. Muñoz, and R. J. Needs, Rev. Mod. Phys. **79**, 863 (2003)

[17] K. Parlinski, computer code PHONON, http://wolf.ifj.edu.pl/phonon

[18] I. Guedes, Y. Hirano, M. Grimsditch, N. Wakabayashi, C. K. Loong, and L. A. Boatner, J. Appl. Phys. **90**, 1843 (2001).

[19] A. B. Garg, R. Rao, T. Sakuntala, B. N. Wani, and V. Vijayakumar, J. Appl. Phys. **106**, 063513 (2009).

[20] C. C. Santos, E. N. Silva, A. P. Ayala, and I. Guedes, J. Appl. Phys. **101**, 053511 (2001).

[21] F. X. Zhang, J. W. Wang, M. Lang, J. M. Zhang, and R. C. Ewing, Phys. Rev. **B 80**, 184114 (2009).

[22] J. A. Tossell, J. Am. Chem. Soc. 97, 4840 (1975).

[23] R. Rao, A. B. Garg, T. Sakuntala, S. N. Achary, and A. K. Tyagi, J. Solid. State Chem. **182**, 1879 (2009).

[24] S. J. Duclos, A. Jayaraman, G. P. Espinosa, A. S. Cooper, and R. G. Maines, J. Phys. Chem. Solids **50**, 769 (1989).

[25] F. D. Hardcastle, and I. E. Wachs, J. Phys. Chem. **95,** 5031 (1991).

[26] I. D. Brown, K. K. Wu, Acta Cryst. **B 32**, 1957 (1976).

[27] D. L. Rousseau, R. P. Baumann, and S. P. Porto, J. Raman Spectrosc. **10**, 253 (1981).

[28] R. Mittal, A. B. Garg, V. Vijaykumar, S. N. Achary, A. K. Tyagi, B. K. Godwal, E. Busetto, A. Lausi, and S. L. Chaplot, J. Phys. Condens. Matter **20**, 075223 (2008).

[29] F. J. Manjón, D. Errandonea, N. Garro, J. Pellicer-Porres, P. Rodríguez Hernández, S. Radescu, J. López-Solano, A. Mujica, and A. Muñoz, Phys. Rev. **B 74**, 144111 (2006).

[30] F. J. Manjón, D. Errandonea, N. Garro, J. Pellicer-Porres, J. López-Solano, P. Rodríguez Hernández, S. Radescu, A. Mujica, and A. Muñoz, Phys. Rev. **B 74**, 144112 (2006).

[31] V. Panchal, N. Garg, and S. M. Sharma, J. Phys. Condens. Matter **18**, 3917 (2008).

[32] R. Lacomba-Perales, D. Martínez-García, D. Errandonea, Y. Le Godec, J. Phillipe3, G. Le Marchand, J.C. Chervin, A. Polian, A. Muñoz, and J. Lopez-Solano, Phys. Rev. B **80**, 144117 (2010).

[33] O. Tschauner, D. Errandonea, and G. Serghiou, Physica B **371**, 88 (2006).

[34] D. Errandonea, R. S. Kumar, X. Ma, and C. Y. Tu, J. Solid State Chem. **181**, 355 (2008).

[35] D. Errandonea, D. Santamaria-Perez, V. Grover, S. N. Achary, and A. K. Tyagi, J. Appl. Phys. **108**, 073518 (2010).

[36] D. Errandonea, D. Santamaria-Perez, T. Bondarenko, and O. Khyzhun, Mater. Res. Bull. **45**, 1732 (2010).

[37] M. Marqués, M. Florez, J. M. Recio, L. Gerward, and J. Staun Olsen, Phys. Rev. **B 74**, 014104 (2006).

[38] R. Lacomba-Perales, D. Errandonea, Y. Meng, and M. Bettinelli, Phys. Rev. **B 81**, 064113 (2010).

[39] Y. W. Long, W. W. Zhang, L. X. Yang, Y. Yu, R. C. Yu, S. Ding, Y. L. Liu, and C. Q. Jin, Appl. Phys. Lett. **87**, 181901 (2005).

[40] Y. W. Long, L. X. Yang, Y. Yu, F. Y. Li, R. C. Yu, S. Ding, Y. L. Liu, and C. Q. Jin, Phys. Rev. **B 74**, 054110 (2006).

[41] D. Errandonea, R. S. Kumar, L. Gracia, A. Beltrán, S. N. Achary, and A. K. Tyagi, Phys. Rev. B **80**, 094101 (2009).

[42] L. Gracia, A. Beltrán, and D. Errandonea, Phys. Rev. **B 80**, 094105 (2009).

[43] D. Errandonea, EPL **77**, 56001 (2007).

[44] D. Errandonea, and F. J. Manjón, Mat. Res. Bull. **44**, 807 (2009).

[45] D. Errandonea, J. Pellicer-Porres, F. J. Manjón, A. Segura, Ch. Ferrer-Roca, R. S. Kumar, O. Tschauner, P. Rodríguez Hernández, J. López-Solano, S. Radescu, A. Mujica, A. Muñoz, and G. Aquilanti, Phys. Rev. **B 72**, 174106 (2005).

[46] D. Errandonea, Phys. Status Solidi **B 242**, R125 (2005).

[47] G. M. Begun, G. W. Beall, L. A. Boatner, and W. J. Gregor, J. Raman Spectrosc. **11**, 273 (1981).

[48] R. Podor, Eur. J. Mineral. **7**, 1353 (1995).

[49] V. Panchal, *et. al*, to be published.

[50] C. C Zhang, Z. M. Zhang, R. C. Dai, Z. P. Wang, J. W. Zhang, and Z. J. Ding, J. Phys. Chem. C **114**, 18279 (2010).

[51] Y. K. Voronko, A. A. Sobol, V. E. Shukshin, A. I. Zagumennyi, Y. D. Zavartsev, and S. A. Kutovoi, Physics of the Solid State **51**, 1886 (2009).

[52] V. E. J. Baran, M. E. Escobar, L. L. Fournier, and R. R. Filgueira, Z. Anorg. Allg. Chem. **472**, 193 (1981).

[53] R. L. Frost, D. A. Henry, M. L. Weier, and W. Martens, J. Raman Spectroscopy **37**, 722 (2006).

[54] J. L. Blin, A. L. Rubbens, F. Wallart, and J. P. Wignacourt, J. Mater. Chem. **6**, 385 (1996).

[55] F. J. Manjón, D. Errandonea, J. López-Solano, P. Rodríguez Hernández, and A. Muñoz, J. Appl. Phys. **105**, 094321 (2009).

[56] S. Tokunaga, H. Kato, and A. Kudo, Chem. Mater. **13**, 4624 (2001).

[57] C. E. Rice and W. R. Robinson, Acta Crystallogr. B: Struct. Crystallogr. Cryst. Chem. **32**, 2232 (1976).

[58] D. Errandonea, F. J. Manjón, M. Somayazulu, and D. Häusermann, J. Solid State Chem. **177**, 1087 (2004).

Table I: *Ab initio* calculated and experimental frequencies at ambient conditions, pressure coefficients, and mode Grüneisen parameters of the $ScVO_4$ in zircon phase. For obtaining mode Grüneisen parameter, $\gamma = (B_0/\omega_0)\times d\omega/dP$ the bulk modulus B_0 = 178 GPa is taken from Ref. 5.

Raman Mode Symmetry	ω_0[a] [cm^{-1}]	$\frac{d\omega}{dp}$[a] [cm^{-1}/GPa]	ω_0[b] [cm^{-1}]	$\frac{d\omega}{dp}$[b] [cm^{-1}/GPa]	γ[b]
$T(E_g)$	109.3	1.01	119.3	0.89	1.33
$T(E_g)$	159.5	-0.18	165.6	-0.05	-0.05
$T(B_{1g})$	163.2	3.72	180.5	2.42	2.39
$\nu_2(B_{2g})$	255.6	-1.37	263.2	-1.15	-0.78
$T(B_{1g})$	263.2	2.68	-----	-----	----
$R(E_g)$	281.6	6.69	304.8	6.28	3.67
$\nu_2(A_{1g})$	326.5	2.15	356.7	2.06	0.94
$\nu_4(E_g)$	377.7	0.82	-----	-----	----
$\nu_4(B_{1g})$	462.5	2.39	494.1	2.62	0.94
$\nu_3(B_{1g})$	827.6	5.78	817.1	5.79	1.26
$\nu_3(E_g)$	848.7	5.78	856.5	5.31	1.10
$\nu_1(A_{1g})$	905.6	5.33	914.2	5.61	1.09

[a] Theoretical calculations
[b] Experimental data

Table II: *Ab initio* calculated and experimental frequencies at ambient conditions, pressure coefficients, and mode Grüneisen parameters of the $ScVO_4$ in scheelite phase. For obtaining mode Grüneisen parameter, $\gamma = (B_0/\omega_0)\times d\omega/dP$ the bulk modulus B_0 = 210 GPa is taken from Ref. 5.

Raman Mode Symmetry	ω_0 [a] [cm^{-1}]	$\frac{d\omega}{dp}$ [a] [cm^{-1}/GPa]	ω_0 [b] [cm^{-1}]	$\frac{d\omega}{dp}$ [b] [cm^{-1}/GPa]	γ [b]
$T(B_g)$	172.8	-0.19	-----	-----	----
$T(E_g)$	178.5	1.56	177.5	3.18	3.76
$T(B_g)$	207.8	3.51	191.3	1.96	2.15
$T(E_g)$	222.5	2.84	213.1	1.62	1.59
$\nu_2(A_g)$	239.6	2.17	257.0	1.87	1.53
$R(A_g)$	318.7	1.71	-----	-----	----
$R(E_g)$	330.4	2.92	336.0	1.55	0.97
$\nu_2(B_g)$	338.2	3.52	363.2	3.62	2.09
$\nu_4(B_g)$	425.3	2.62	449.0	2.11	0.99
$\nu_4(E_g)$	425.7	3.35	456.0	4.68	2.16
$\nu_3(E_g)$	755.8	3.75	727.5	0.41	0.12
$\nu_3(B_g)$	793.9	3.05	760.9	2.53	0.69
$\nu_1(A_g)$	809.3	3.42	826.1	3.72	0.95

[a] Theoretical calculations
[b] Experimental data

Table III: *Ab initio* calculated frequencies at 23.3 GPa and experimental frequencies at 23.4 GPa and pressure coefficients of the $ScVO_4$ in the fergusonite phase.

Raman Mode Symmetry	ω [a] [cm^{-1}]	$\frac{d\omega}{dp}$ [a] [cm^{-1}/GPa]	ω [b] [cm^{-1}]	$\frac{d\omega}{dp}$ [b] [cm^{-1}/GPa]
B_g	204.3	1.55	-----	
A_g	208.7	1.97	228.2	1.83
B_g	237.4	2.19	252.0	2.43
A_g	266.5	1.28	278.6	1.44
B_g	296.2	1.43	311.3	1.27
B_g	302.1	3.69	-----	-----
A_g	311.8	0.89	-----	-----
A_g	358.7	1.98	-----	-----
B_g	379.5	1.48	382.4	1.89
A_g	425.9	2.96	-----	-----
B_g	441.9	2.09	454.3	2.54
B_g	482.4	2.33	505.4	2.21
B_g	515.4	3.04	557.0	2.54
A_g	536.2	3.44	565.9	2.74
A_g	753.2	1.12	776.0	1.85
B_g	773.7	2.41	800.9	2.46
B_g	836.7	2.05	838.8	2.18
A_g	917.6	2.55	935.3	2.62

[a] Theoretical calculations
[b] Experimental data

Table IV: Symmetric stretching frequency at ambient pressure ω_0 of the $\nu_1(A_g)$ mode for various AVO_4 vanadates in both zircon and scheelite phases as a function of their A ionic radius (Shannon radius), r_A.

Compound	r_A [Å]	ω_0 [a] [cm^{-1}]	ω_0 [b] [cm^{-1}]	References
$ScVO_4$	0.87	914	826	This work
$LuVO_4$	0.977	901	830	[23]
$YbVO_4$	0.985	901	823	[19, 20]
$TmVO_4$	0.994	894		[20]
$ErVO_4$	1.004	890		[20]
$HoVO_4$	1.015	891		[20]
YVO_4	1.019	891	829	[7]
$DyVO_4$	1.027	889	825	[24]
$TbVO_4$	1.04	882	829	[24]
$GdVO_4$	1.053	884	830	[50, 51]
$EuVO_4$	1.066	871		[52]
$SmVO_4$	1.079	877		[20]
$NdVO_4$	1.109	871	828	[49]
$PrVO_4$	1.126	869		[20]
$CeVO_4$	1.143	859	826	[20, 49]
$LaVO_4$	1.16	860		[20]
$BiVO_4$	1.17	858	828	[53, 54]

[a] Zircon phase

[b] Scheelite phase

Table V: Zircon to scheelite phase transition pressure, P_T, for various AVO_4 vanadates as a function of the *A* cation ionic radius (Shannon radius), r_A.

Compound	r_A [Å]	P_T [GPa]	References
$ScVO_4$	0.87	8.5	This work
$LuVO_4$	0.977	8.0	[23]
$YbVO_4$	0.985	5.9	[19]
YVO_4	0.95	7.5	[7]
$DyVO_4$	1.027	6.6	[24]
$TbVO_4$	1.04	6.5	[24]
$GdVO_4$	1.053	6.3	[50]
$NdVO_4$	1.109	5.9	[49]
$CeVO_4$	1.143	5.0	[49]

Figure Captions:

Fig. 1: (a) Raman spectra of $ScVO_4$ in the zircon phase between 1 atm and 7.6 GPa. Asterisks represents the second order Raman modes. (b) Pressure dependence of the Raman-mode frequencies in zircon-type $ScVO_4$ (solid symbols). Empty symbols are likely second-order Raman modes. The solid lines are the calculated modes. The dashed lines represent Raman modes not observed in the experiments.

Fig. 2: (a) Raman spectra of the scheelite phase of $ScVO_4$ at pressures between 8.5 GPa and 16.5 GPa on upstroke and between 9.9 GPa and 0.2 GPa on downstroke (b) Experimental pressure dependence of the Raman-mode frequencies in scheelite- and fergusonite-type $ScVO_4$. Filled and empty circles correspond to Raman modes in scheelite-type $ScVO_4$ during upstroke and downstroke, respectively. Filled and empty squares correspond to Raman modes in fergusonite-type $ScVO_4$ on upstroke and downstroke, respectively. Filled triangles are likely second-order modes of the scheelite phase. The solid lines are the calculated modes. The dashed lines represent Raman modes not observed in the experiments.

Fig. 3: Raman spectra of the HP fergusonite phase of $ScVO_4$ between 18.2 GPa and 35 GPa. The Raman spectra of scheelite phase at 16.5 GPa is also shown for comparison. Arrows show the two modes that exhibit considerably broadening upon compression.

Fig. 4: FWHM of the mode assigned to the $\nu_3(E_g)$ in the scheelite phase between 9.7 GPa and 35 GPa. The broadening beyond 18.2 GPa evidences the phase transition.

Fig. 5: (a) Experimental symmetric stretching $\nu_1(A_g)$ frequencies in the zircon and scheelite phases for various AVO_4 vanadates as a function of the A cation ionic radius,

r_A. Circles correspond to zircon phase and square correspond to scheelite phase. The dashed lines are linear fit of the experimental data. (b) Plot of the zircon to scheelite transition pressure for various AVO_4 vanadates as a function of the A cation ionic radius, r_A. The dashed line is linear fit of the experimental data.

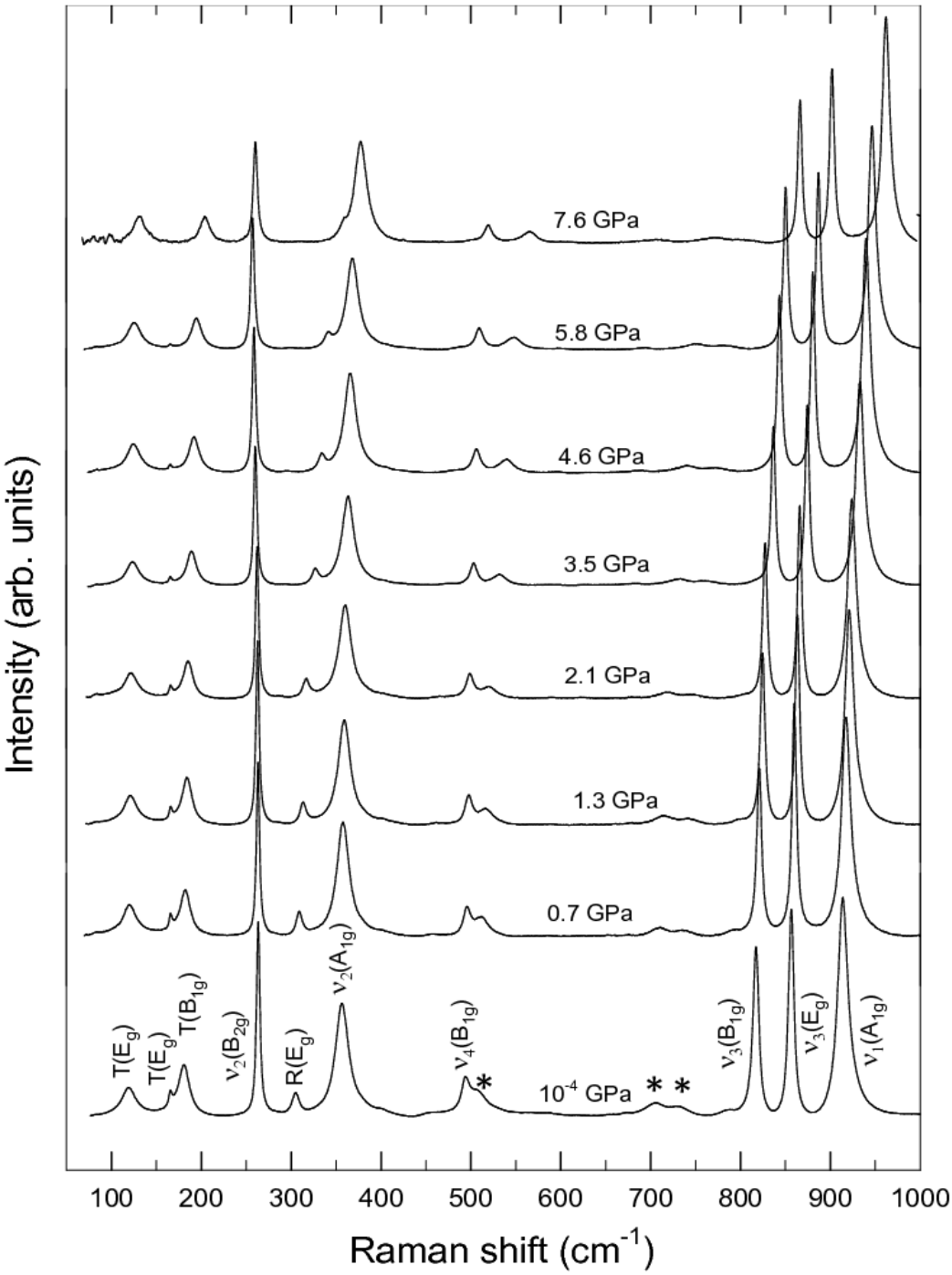
7.6 GPa
5.8 GPa
4.6 GPa
3.5 GPa
2.1 GPa
1.3 GPa
0.7 GPa
10-4 GPa
T(Eg)
T(Eg)
T(B1g)
ν2(B2g)
R(Eg)
ν2(A1g)
ν4(B1g)
ν3(B1g)
ν3(Eg)
ν1(A1g)
Intensity (arb. units)
Raman shift (cm-1)
100
200
300
400
500
600
700
800
900
1000

Figure 1(a)

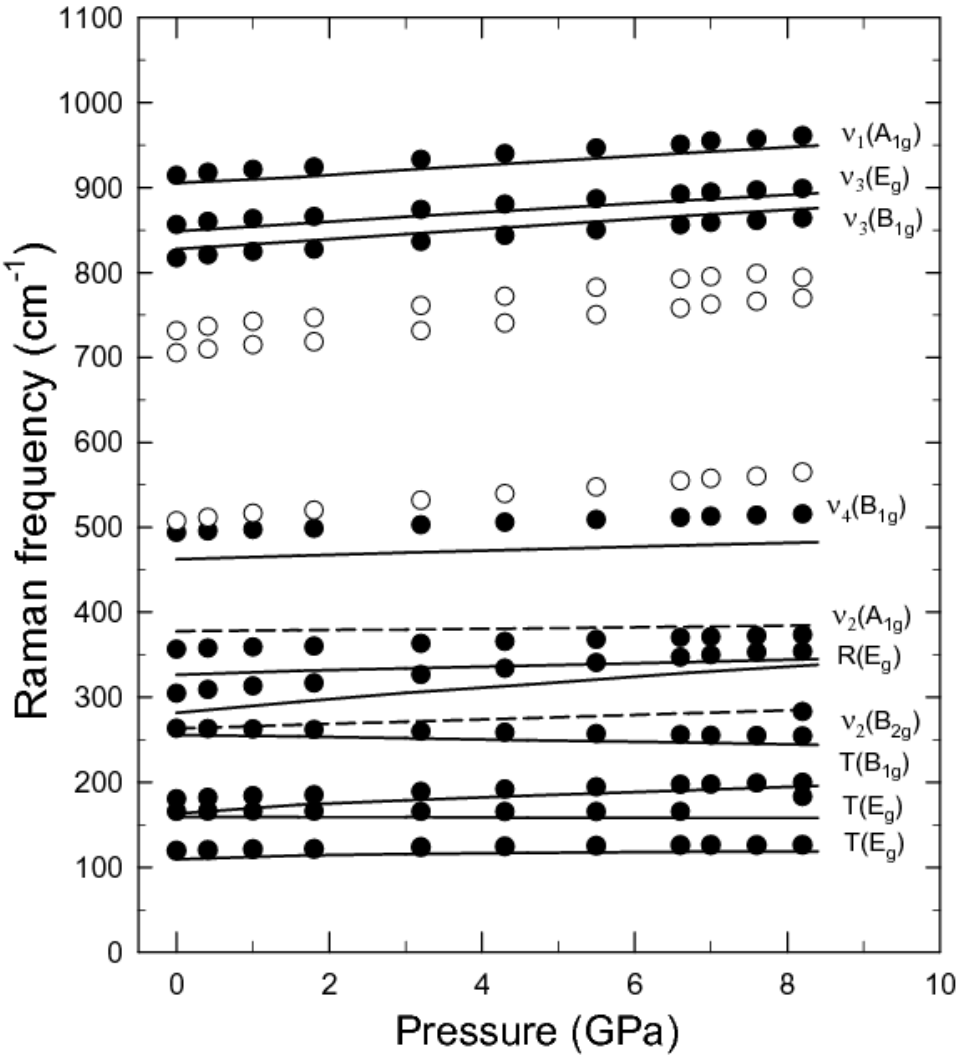
Raman frequency (cm^{-1})
Pressure (GPa)
$\nu_1(A_{1g})$
$\nu_3(E_g)$
$\nu_3(B_{1g})$
$\nu_4(B_{1g})$
$\nu_2(A_{1g})$
$R(E_g)$
$\nu_2(B_{2g})$
$T(B_{1g})$
$T(E_g)$
$T(E_g)$

Figure 1(b)

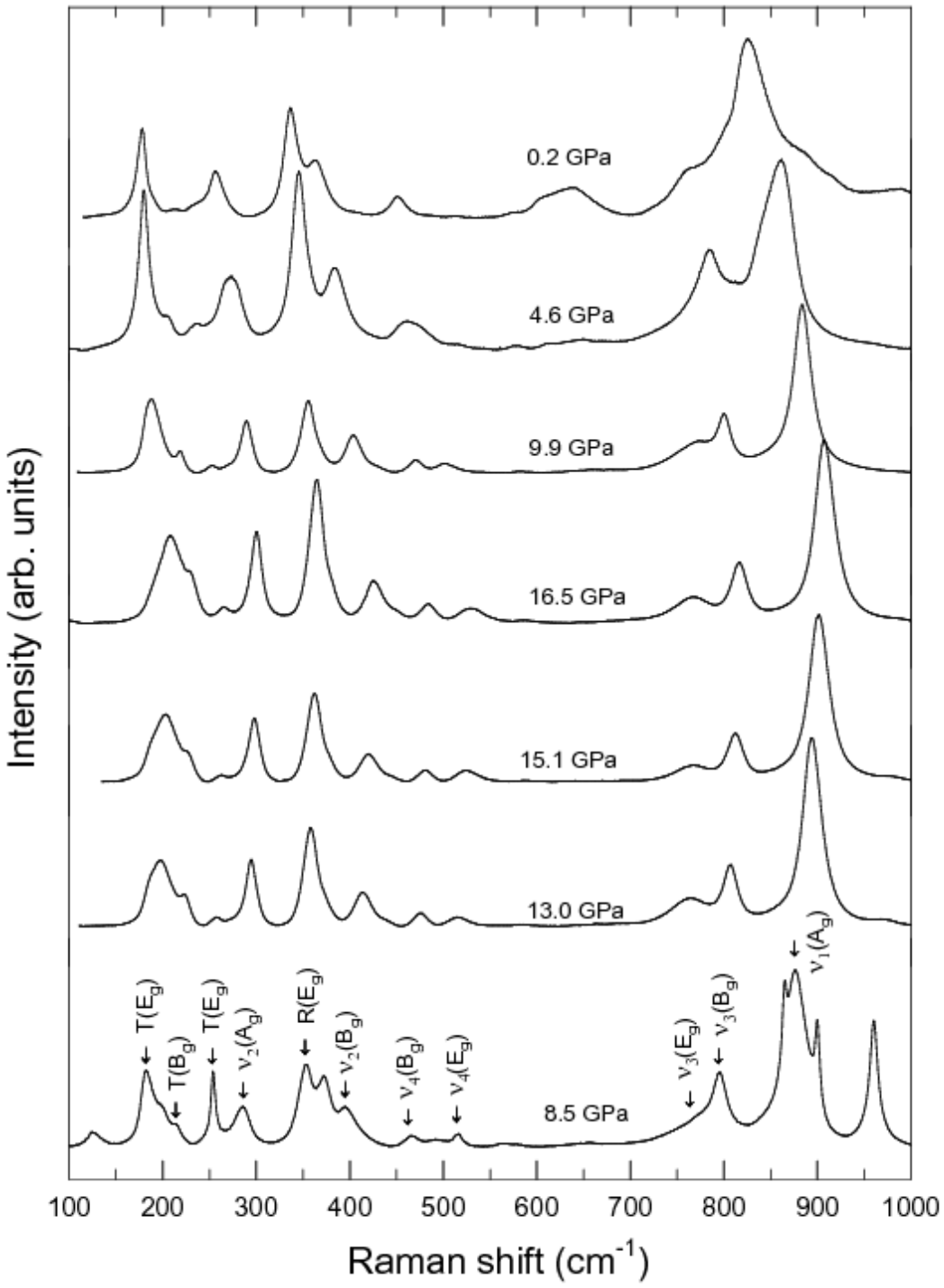
0.2 GPa
4.6 GPa
9.9 GPa
16.5 GPa
15.1 GPa
13.0 GPa
8.5 GPa
T(Eg)
T(Bg)
T(Eg)
ν2(Ag)
R(Eg)
ν2(Bg)
ν4(Bg)
ν4(Eg)
ν3(Eg)
ν3(Bg)
ν1(Ag)
Intensity (arb. units)
100
200
300
400
500
600
700
800
900
1000
Raman shift (cm-1)

Figure 2(a)

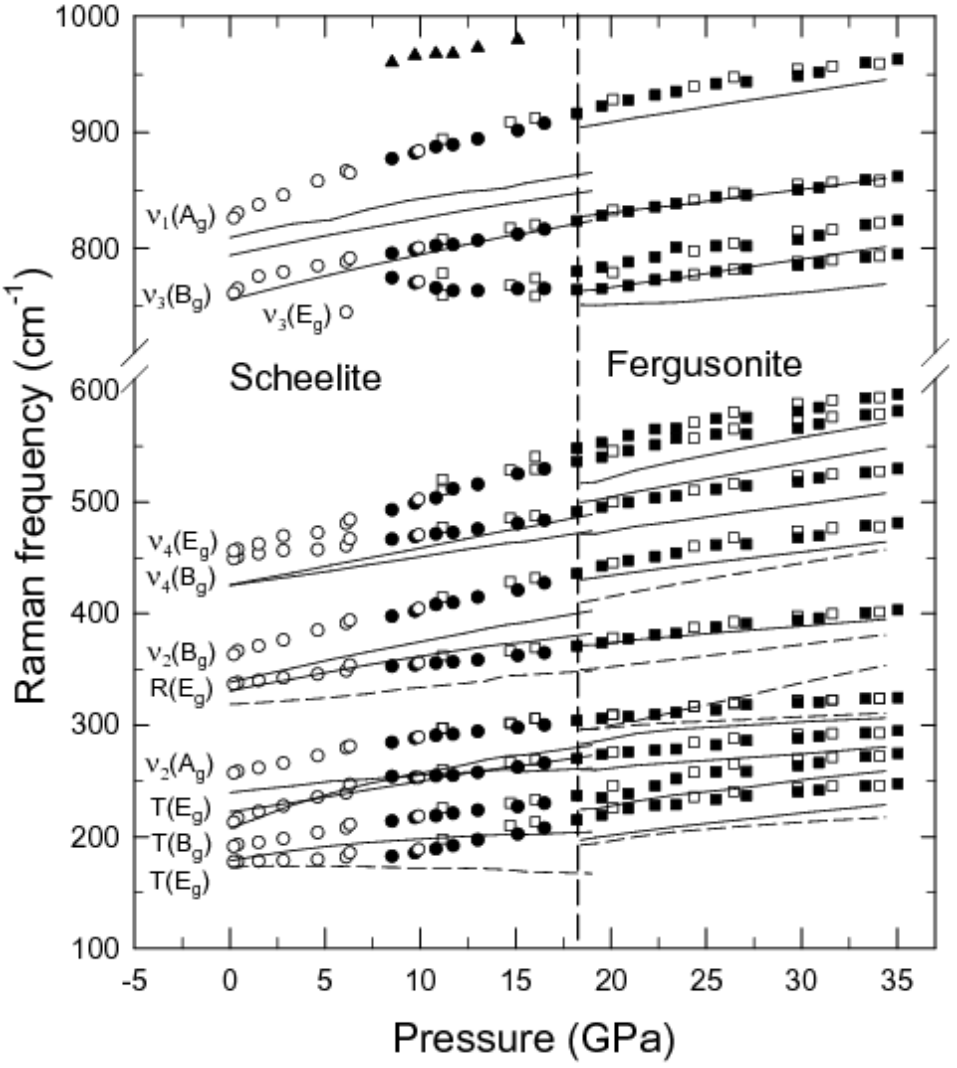
Raman frequency (cm^{-1})
Pressure (GPa)
Scheelite
Fergusonite
$\nu_1(A_g)$
$\nu_3(B_g)$
$\nu_3(E_g)$
$\nu_4(E_g)$
$\nu_4(B_g)$
$\nu_2(B_g)$
R(E_g)
$\nu_2(A_g)$
T(E_g)
T(B_g)
T(E_g)
1000
900
800
600
500
400
300
200
100
-5
0
5
10
15
20
25
30
35

Figure 2(b)

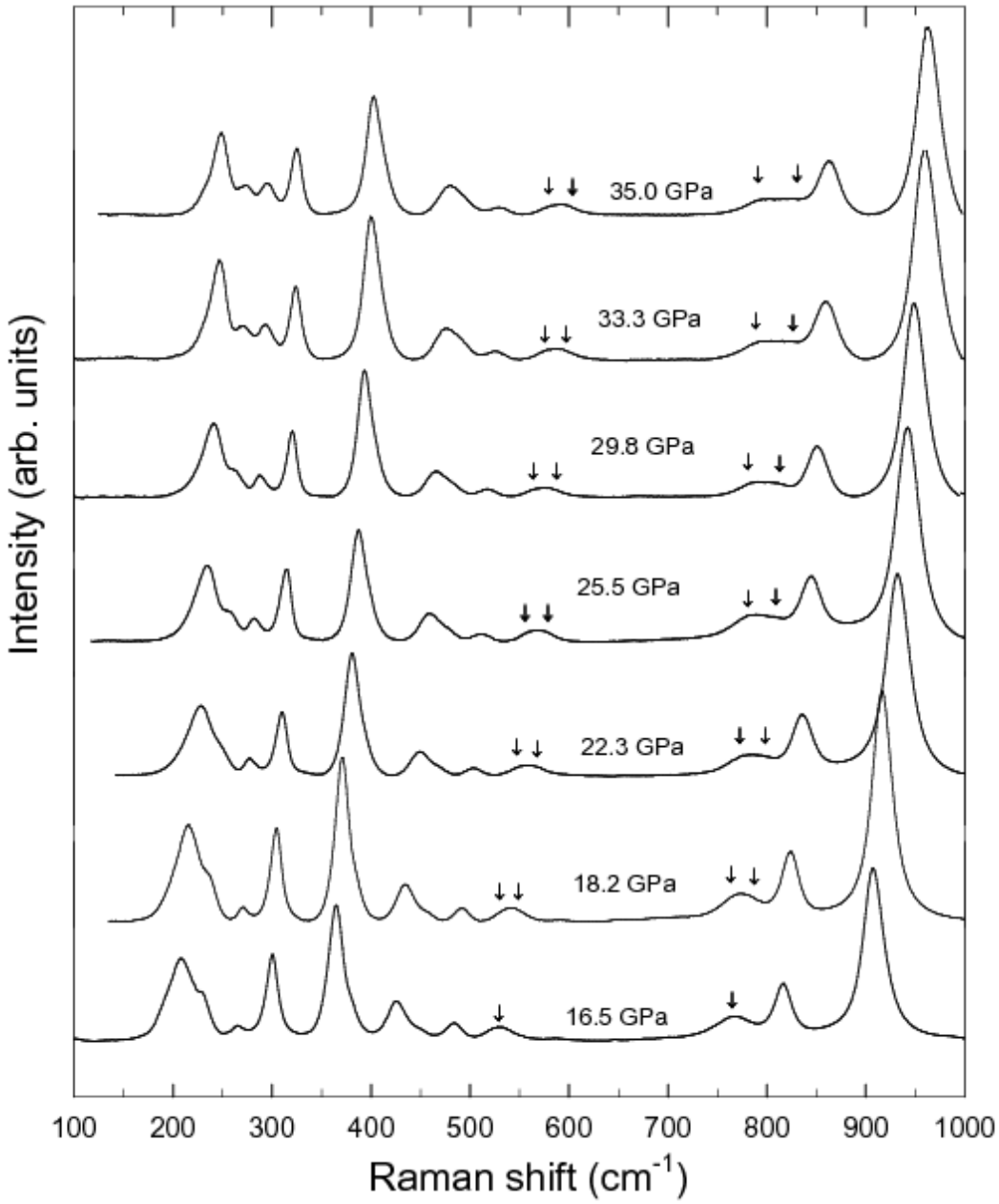
35.0 GPa
33.3 GPa
29.8 GPa
25.5 GPa
22.3 GPa
18.2 GPa
16.5 GPa
Intensity (arb. units)
100
200
300
400
500
600
700
800
900
1000
Raman shift (cm-1)

Figure 3

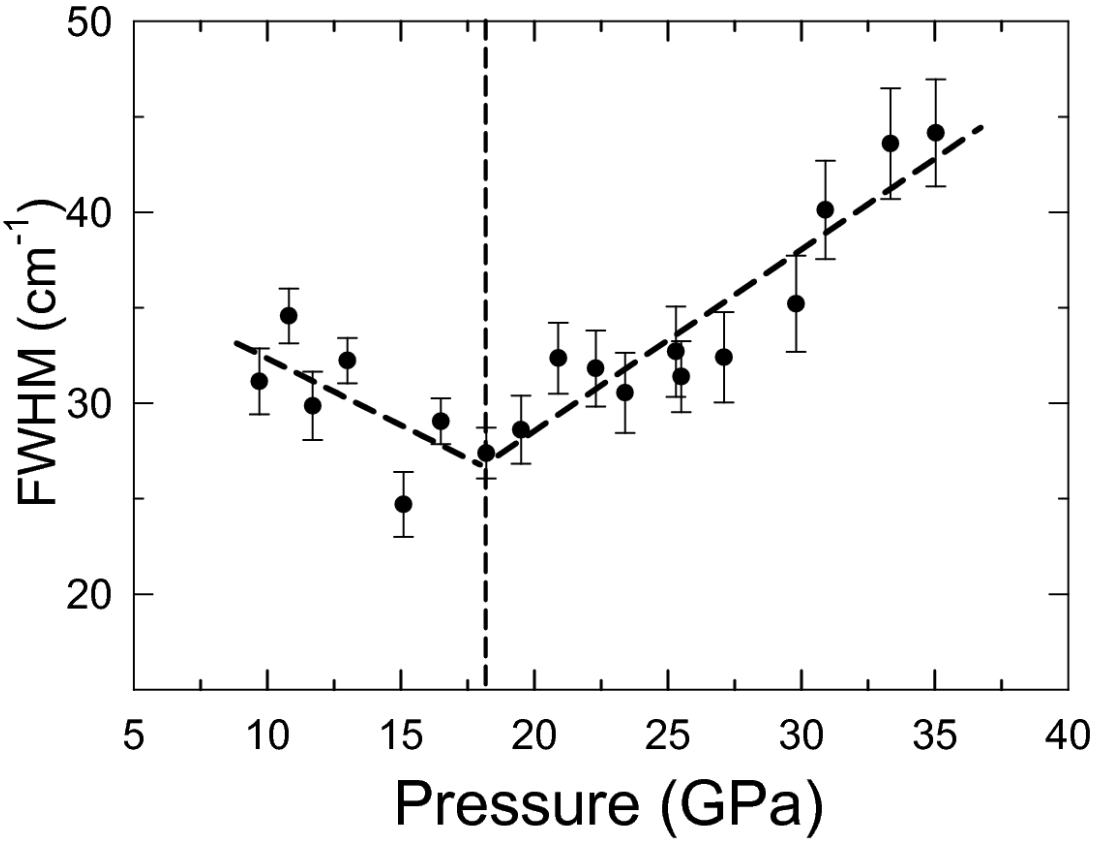

Figure 4

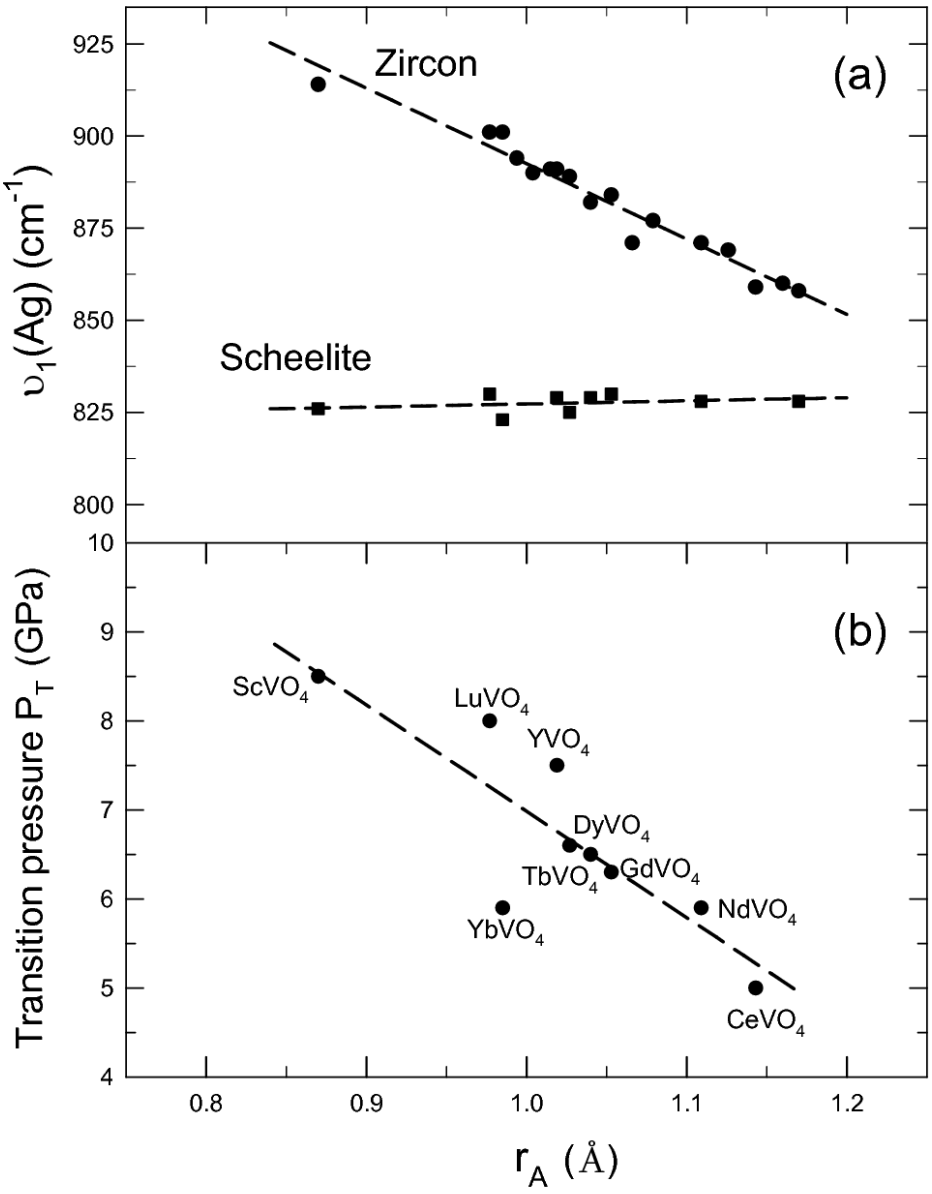
Zircon
(a)
Scheelite
υ_1(Ag) (cm^{-1})
925
900
875
850
825
800
(b)
ScVO$_4$
LuVO$_4$
YVO$_4$
DyVO$_4$
TbVO$_4$
GdVO$_4$
NdVO$_4$
YbVO$_4$
CeVO$_4$
Transition pressure P$_T$ (GPa)
10
9
8
7
6
5
4
0.8
0.9
1.0
1.1
1.2
r$_A$ (Å)

Figure 5